

## ARTICLE OPEN



# Dynamic manipulation of microwave polarization based on anisotropic graphene meta-device

Jin Zhang<sup>1</sup>, Zhenfei Li<sup>1</sup>, Chiben Zhang<sup>1,2</sup>, Linda Shao<sup>1</sup> and Weiren Zhu<sup>1</sup>✉

As a unique two-dimensional atomic material, graphene offers excellent mechanical properties, dynamically tunable surface conductivity, ultra-high carrier mobility, and optical transparency, making it great potential for novel electromagnetic devices. However, dynamic manipulation of microwave polarization has not been experimentally realized in a graphene-assisted metasurface. In this paper, we present a general strategy for designing graphene-based active meta-device for achieving dynamic polarization control at microwave frequencies. When illuminated by a linear-polarized incident wave, the polarization angle of the reflected wave can be dynamically controlled by shifting the bias voltage applied to graphene. The simulated and measured results reveal that the proposed graphene-based meta-device offers a novel approach to the manipulation of microwave polarization and has potential applications in antenna, sensing, and communications.

npj 2D Materials and Applications (2022)6:47; https://doi.org/10.1038/s41699-022-00322-8

## INTRODUCTION

During the past decades, metasurfaces, referred to as the two-dimensional (2D) version of metamaterials, have experienced a great upsurge in various scientific and engineering disciplines due to their intriguing and tailorable properties that are not naturally available<sup>1–3</sup>. In contrast to the traditional bulk metamaterials, metasurfaces possess many attractive features such as easy fabrication, low profile, and low loss that triggered an enormous outburst of novel research in electromagnetic cloaking<sup>4</sup>, holographic imaging<sup>5,6</sup>, information processing<sup>7,8</sup>, to name a few. By designing and arranging the individual sub-wavelength meta-atoms in desired ways, metasurfaces provide an unprecedented degree of freedom in engineering light-matter interactions at the sub-wavelength scale, achieving complete control over the phase, amplitude, frequency, polarization, and propagation direction of electromagnetic waves<sup>9–12</sup>. In particular, polarization state is one of the intrinsic characteristics of electromagnetic waves which plays a role of paramount importance in many areas, such as display optics<sup>13</sup>, quantum computation<sup>14</sup>, chemical sensing<sup>15</sup>, and so on. Due to the invariance and independence of polarization on time and frequency domains, polarization modulation is compatible with other modulation techniques that are of central interest in wireless communication and radar systems<sup>16</sup>. Standard approaches for traditional polarization control technology involve the Faraday effect and natural birefringent crystals<sup>17,18</sup>. Due to the extremely weak electromagnetic responses from natural materials, high thickness or external magnetic field is usually required to obtain phase accumulation, which is confronted with limited bandwidth and bulky volume. In contrast, metasurfaces have shown unparalleled capabilities for flexibly controlling polarization in a planar and integrated manner, providing a novel platform for versatile polarization transformations<sup>19,20</sup>, polarization gratings<sup>21</sup>, holography and imaging<sup>22,23</sup>, etc.

The manipulation of polarization using metasurfaces generally relies on the structurally varying anisotropy, i.e., shape, size, and orientation of the comprised meta-atoms, which can modify the two orthogonally polarized components of the incident electromagnetic

wave independently and thus generate desired output polarization via vector superposition. In recent years, metasurface-assisted polarization modulators/converters have been intensively investigated from gigahertz<sup>24,25</sup>, terahertz<sup>26,27</sup>, to optical regions<sup>28,29</sup>. However, the functionalities of metasurfaces are fixed once the geometric structures are designed and fabricated, limiting their practical applications. An effective way to overcome such limitation is to employ tunable metasurfaces, whose electromagnetic responses can be actively controlled through integration with active materials or elements. Various types of tunable metasurfaces have been experimentally realized at microwave frequencies with active elements such as PIN diodes, varactors, or semiconductors for real-time control of the meta-atoms by external bias voltages<sup>30–32</sup>. However, complex bias network, welding deformations, poor flexibility, and high cost of loading active components still face tremendous challenges in practical applications<sup>33</sup>. Fortunately, as a 2D material consisting of carbon atoms arranged in a honeycomb lattice, graphene is a promising candidate for reconfigurable devices, owing to its surface conductivity enables dynamically controlled in a wide band by electrical biasing or chemical doping<sup>34–36</sup>. Thus, the integration of graphene in metasurfaces has been successfully enforced into universal devices for polarization modulation in terahertz or infrared frequencies<sup>37–40</sup>. The basic idea of these works is attributed to the anisotropic patterns of graphene or hybrid graphene/metal structures that support tunable plasmonic eigenmodes along the two orthogonal polarization directions, relying on the dynamic shifts of resonances. Shvet et al. proposed a novel method for measuring the polarization state of incident light using graphene-integrated anisotropic metasurfaces in the far-infrared region<sup>41</sup>. While in the microwave region, graphene behaves more like a purely resistive film and its reactance is fixed to nearly zero. As a consequence, the realization of tunable resonances at microwave frequencies is significantly different from that at higher frequencies<sup>42–44</sup>. Until now, only a few attempts have been devoted to the passive polarization modulation of microwaves using graphene. Grande et al. achieved SOCL<sub>2</sub>-doped multilayer graphene with a sheet resistance value below 30 Ω□<sup>-1</sup> and exploited it for the

<sup>1</sup>Department of Electronic Engineering, Shanghai Jiao Tong University, Shanghai 200240, P. R. China. <sup>2</sup>Air and Missile Defense College, Air Force Engineering University, Xi'an 710051, P. R. China. ✉email: weiren.zhu@sjtu.edu.cn

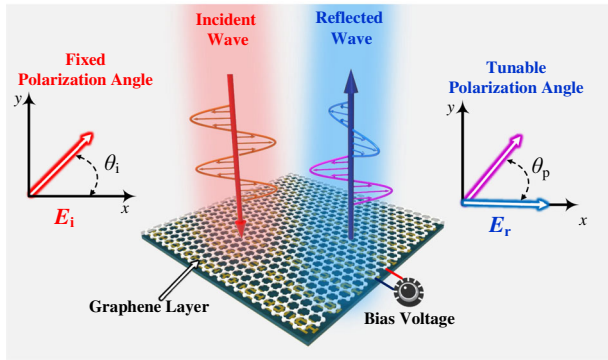


**Fig. 1 Working principle of the proposed graphene-based meta-device.** The proposed meta-device is capable of dynamically rotating the polarization angle of incident waves.

realization of an optically transparent polarizer<sup>45</sup>. Chen et al. demonstrated a microwave polarization converter based on graphene ribbon metasurface, where the full polarization transformation including linear-to-linear, linear-to-circular, and linear-to-elliptical conversions are realized by properly selecting the surface impedance of graphene<sup>46</sup>. Recently, Zhang et al. proposed a graphene-based meta-filter in microwave band enabling decomposition and manipulation of arbitrary incoming polarized states such as linear-, circular-, and even elliptical polarization<sup>47</sup>. However, only passive control of polarization has been experimentally realized in these works without taking advantage of graphene's electrical tunability. Until now, graphene-based microwave metasurfaces with real-time polarization tunability have not been reported yet.

In this paper, we present a novel design of graphene-based meta-device with a dynamically tunable polarization state at microwave frequencies for the first time to our best knowledge. Combining metallic resonators with graphene-based sandwich layers (GSL), the anisotropic amplitude modulation accompanied by zero phase difference between  $x$ - and  $y$ -polarized reflected waves is achieved, which enables dynamical manipulation of polarization controlled by the tunable sheet resistance of graphene. Moreover, experimental results demonstrate the relationship between the polarization angle and the varying biasing voltage applied to the graphene layers, showing that graphene has great potential for microwave polarization manipulations, which has great prospects in antennas and wireless communications.

## RESULTS AND DISCUSSION

### Design of graphene-based meta-device

The working principle of the proposed graphene-based meta-device is illustrated in Fig. 1. Gate-controlled GSL and metallic resonators are employed to construct the proposed meta-device. In contrast to the conventional scheme of active electronic elements driven by a field-programmable gate array, graphene is introduced to realize the anisotropic amplitude modulation of electromagnetic waves in a simpler manner. Therefore, the proposed meta-device is capable of dynamically rotating the polarization angle of incident waves. By applying a different bias voltage to the graphene layers, the polarization angle of the reflected wave  $\theta_p$  can be continuously and dynamically rotated from  $0^\circ$  to  $45^\circ$ .

The proposed meta-device, as shown in Fig. 2a, consists of five layers: a GSL on the top, a foam layer, a patterned layer of metallic resonator, a substrate layer, and a metallic ground at the bottom. The GSL is composed of two monolayer graphene sheets transferred on a 0.2-mm-thick polyethylene terephthalate (PET)

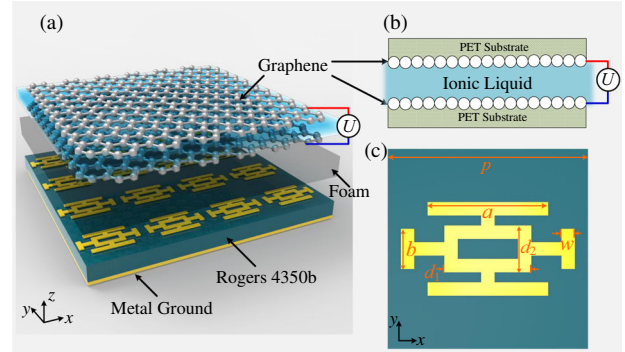


**Fig. 2 Schematic diagram of the proposed graphene-based meta-device.** **a** Schematic view of the proposed meta-device. **b** Side view of GSL and **c** top view of metallic periodic cross-shaped resonator. Geometric parameters are  $p = 6$  mm,  $w = 0.4$  mm,  $a = 3.6$  mm,  $b = 1.2$  mm,  $d_1 = 2.6$  mm, and  $d_2 = 1.4$  mm.

substrate and a 0.05-mm-thick diaphragm paper soaked with ionic liquid electrolyte (1-butyl-3-methylimidazolium hexafluorophosphate) between them<sup>48,49</sup>. This configuration indeed improves the gating feature of graphene<sup>50</sup>. The metallic pattern layer is printed on a 0.762-mm-thick grounded dielectric substrate (Rogers 4350b,  $\epsilon_s = 3.6$ ,  $\tan\delta = 0.0037$ ). To achieve the arbitrary phase coverage and negligible cross-polarized effect in an anisotropic structure, the metallic resonator is designed as a combination of Jerusalem crosses and square loops as shown in Fig. 2b. The four resonant arms and central square loop increase the phase coverage by strengthening the corresponding electric field resonance to achieve additional phase accumulation. Final geometrical parameters of the metal pattern are shown as follows:  $p = 6$  mm,  $w = 0.5$  mm,  $a = 1.25$  mm,  $b = 0.85$  mm,  $d_1 = 2.6$  mm, and  $d_2 = 1.4$  mm. The bottom metallic ground is copper with a conductivity of  $5.8 \times 10^7$  S  $m^{-1}$  and a thickness of 0.035 mm. The 2-mm-thick Teflon foam ( $\epsilon_f = 1.05$ ) is set under the graphene layer to avoid direct contact with metal. Because the thickness of the foam in the middle is much larger than graphene and metallic layers, the whole proposed structure works as an analog of Fabry–Perot cavity that hardly supports the surface plasmon polaritons effect between graphene and metallic layers. The electric property of graphene can be described in terms of a surface conductivity  $\sigma_g$  as given by the well-known Kubo formula<sup>51,52</sup>:

$$\sigma_g = \sigma_{\text{intra}}(\omega, E_F, \Gamma, T) + \sigma_{\text{inter}}(\omega, E_F, \Gamma, T), \quad (1)$$

$$\sigma_{\text{intra}} = -i \frac{e^2 k_B T}{\pi^2 (\omega - i\tau^{-1})} \left[ \frac{E_F}{k_B T} + 2 \ln \left( e^{\frac{E_F}{k_B T}} + 1 \right) \right], \quad (2)$$

$$\sigma_{\text{inter}} \simeq -i \frac{e^2}{4\pi} \ln \left[ \frac{2|E_F| - (\omega - i2\Gamma)}{2|E_F| + (\omega - i2\Gamma)} \right], \quad (3)$$

where  $k_B$  and  $\hbar$  are the Boltzmann constant and the reduced Planck constant (Dirac constant).  $e$  is the electron charge,  $\omega$  is the angular frequency,  $T$  is the temperature and is fixed to 300 K.  $\Gamma = (2\tau)^{-1}$  is the carrier scattering rate in graphene,  $\tau$  is the relaxation time, and  $E_F$  is the Fermi energy. In microwave band, the value of  $\sigma_g$  is mainly defined by the intra-band transitions. Moreover, the resistance term of graphene impedance keeps almost constant and its reactance term tends to zero. Hence, graphene is generally modeled as a resistive planar sheet at the microwave frequencies of our interest and can be characterized by sheet resistance  $R_g$ :

$$R_g = \frac{1}{\sigma_g} \simeq \frac{\pi^2 (\omega + i2\Gamma)}{ie^2 k_B T} \left[ \frac{E_F}{k_B T} + 2 \ln \left( 1 + e^{\frac{E_F}{k_B T}} \right) \right]^{-1}. \quad (4)$$

The sheet resistance of graphene  $R_g$  is determined by the Fermi energy  $E_F$  and the relaxation time  $\tau$ . We assumed  $\tau = 0.2$  ps in this contribution, which is in agreement with measured data of chemical-vapor-deposited (CVD) graphene. On the other hand, when the electrostatic field bias ( $U$ ) is applied to the graphene sandwich structure, the ions in the electrolyte with opposite polarization would be concentrated on the interfaces of the graphene electrodes that enables the electrostatically doping of graphene. Therefore, the Fermi energies of graphene will be dynamically controlled, thus resulting in the variation of sheet resistance<sup>50</sup>.

### Polarization transformation

To theoretically analyze the operating principle of polarization manipulation in the proposed meta-device, we consider a linearly polarized electromagnetic wave that normally illuminates on the planar structure along the  $-z$  direction, whose electric field can be decomposed into two orthogonal components in the Cartesian base:

$$\mathbf{E}_i(\mathbf{r}, t) = \begin{pmatrix} I_x \\ I_y \end{pmatrix} e^{j(\omega t + kz)}, \quad (5)$$

where  $\omega$  is the angular frequency,  $k$  represents the wave vector,  $I_x$  and  $I_y$  are complex amplitudes of incident electric fields along  $x$  and  $y$  axis, respectively. The Jones vector expressed as  $[I_x, I_y]^T = [|E_i| \cos \theta_i, |E_i| \sin \theta_i]^T$  determines the state of polarization and the total intensity of the electromagnetic wave, with  $\theta_i$  representing the angle between  $x$  axis and the direction of the electric field. Similarly, the reflected electromagnetic waves are depicted as:

$$\mathbf{E}_r(\mathbf{r}, t) = \begin{pmatrix} R_x \\ R_y \end{pmatrix} e^{j(\omega t - kz)}, \quad (6)$$

According to the Jones matrix  $\mathbf{J}^{53}$ , the relationship between the incident and reflected electric fields can be expressed as:

$$\begin{pmatrix} R_x \\ R_y \end{pmatrix} = \begin{pmatrix} J_{xx} & J_{xy} \\ J_{yx} & J_{yy} \end{pmatrix} \begin{pmatrix} I_x \\ I_y \end{pmatrix}. \quad (7)$$

Here,  $J_{xy}$  and  $J_{yx}$  are cross-polarized reflection coefficients,  $J_{xx}$  and  $J_{yy}$  represent the co-polarized reflection coefficients in  $x$  and  $y$  direction, respectively. We confirmed that the cross-polarized reflections in our proposed structure are much smaller than the co-polarized reflections (full data are provided in Supplementary Fig. 1 and Supplementary Note 1). Therefore, On the condition without cross-polarization effects ( $J_{xy} = J_{yx} = 0$ ), the reflected field

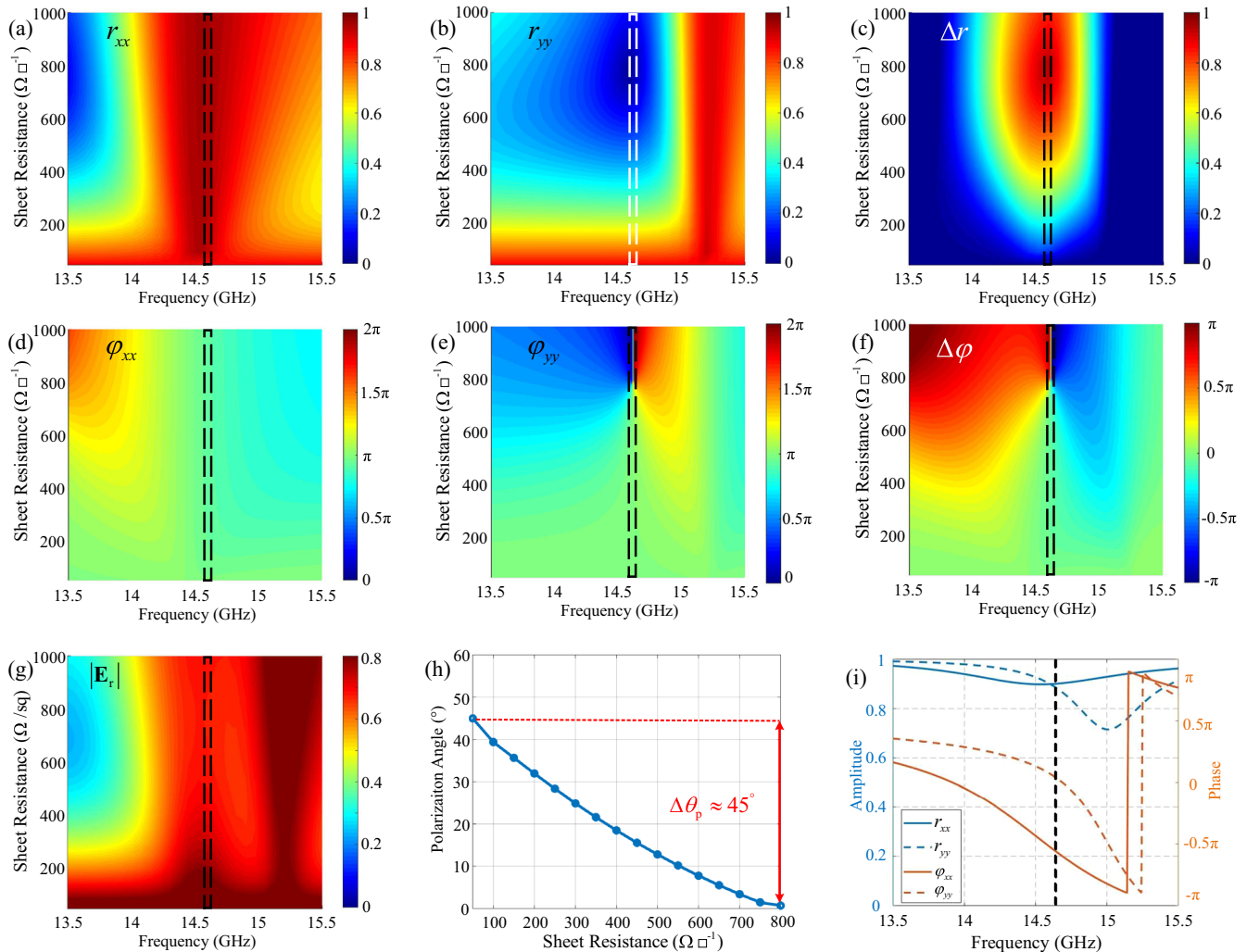


**Fig. 3 Simulated results of graphene-based meta-device.** Simulated reflected amplitude (a, b) and phase spectra (d, e) of the metasurface with a different sheet resistance of graphene under  $x$ - and  $y$ -polarized incident waves. Simulated amplitude (c) and phase difference (f) spectra as a function of sheet graphene's resistance. **g** The intensity spectra of the reflected electric field. **h** The tunable polarization angle for sheet graphene's resistance. **i** Simulated amplitude and phase response of the proposed meta-device without graphene layer.

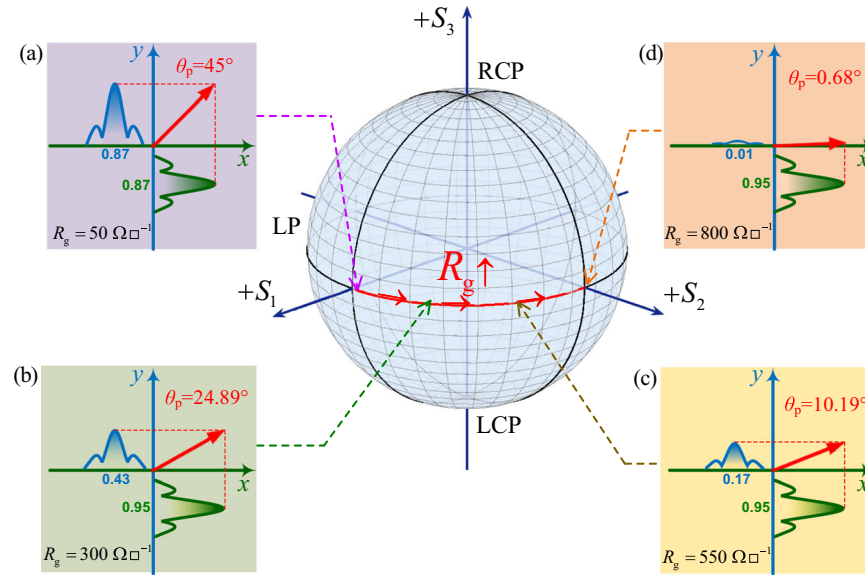


**Fig. 4 Polarization state in the Poincaré sphere.** Four typical polarization states with different linear polarization angles marked in the Poincaré sphere. The surrounding four pictures are the  $x$  and  $y$  components of related simulated electric fields with four different  $R_g$  of **a**  $50 \Omega \square^{-1}$ , **b**  $300 \Omega \square^{-1}$ , **c**  $550 \Omega \square^{-1}$ , and **d**  $800 \Omega \square^{-1}$ .

can be expressed as:

$$\begin{pmatrix} R_x \\ R_y \end{pmatrix} = \begin{pmatrix} J_{xx} & 0 \\ 0 & J_{yy} \end{pmatrix} \begin{pmatrix} I_x \\ I_y \end{pmatrix} = \begin{pmatrix} r_{xx} e^{-j\phi_{xx}} I_x \\ r_{yy} e^{-j\phi_{yy}} I_y \end{pmatrix}, \quad (8)$$

where  $r_{mm}$  and  $\phi_{mm}$  are the amplitude and phase of the reflection coefficient in  $m$  direction. The Jones vector of a linear-polarized plane wave with  $\theta_i = 45^\circ$  can be written as  $[1, 1]^T$  and the reflected field can be written as:

$$\begin{pmatrix} R_x \\ R_y \end{pmatrix} = \begin{pmatrix} r_{xx} e^{-j\phi_{xx}} I_x \\ r_{yy} e^{-j\phi_{yy}} I_y \end{pmatrix}. \quad (9)$$

According to Eq. (8), the polarization state of the resultant reflected electromagnetic wave depends on the amplitude and phase differences of the reflection coefficients between two orthogonal directions, if the Jones vector of the incident wave is set to  $[1, 1]^T$  ( $\theta_i = 45^\circ$ ). For example, the reflected wave is converted to circular polarization when the phase difference between  $\phi_{xx}$  and  $\phi_{yy}$  equals  $0.5n\pi$ , where  $n$  represents an odd number. When satisfying the equation of  $\phi_{xx} = \phi_{yy}$ , the polarization state of the reflected wave will be the same as that of the incident wave. In this case, the intensity of reflected field  $|E_r|$  and polarization angle  $\theta_p$  are determined by amplitude coefficients, which can be expressed as follows:

$$|E_r| = \sqrt{|R_x|^2 + |R_y|^2} = \sqrt{|r_{xx}|^2 + |r_{yy}|^2} \quad (10)$$

$$\theta_p = \arctan \frac{r_{yy}}{r_{xx}} \quad (11)$$

Therefore, dynamic polarization manipulation of the reflected electromagnetic wave can be realized by utilizing an active metasurface if the amplitude or phase components in Jones matrix could be dynamically controlled.

### Simulations

The reflection spectra of the proposed metasurface are simulated and characterized using commercial time-domain software CST Microwave Studio. Unit cell boundary conditions and Floquet ports were set along the  $x$  and  $y$  directions representing a periodical structure, and an open boundary was defined in

$z$  direction for electromagnetic wave incidence and reflection. The simulated amplitude and phase components of the co-polarized reflection coefficients along  $x$  and  $y$  directions are displayed in Fig. 3a, b, d, e. It can be seen that the reflected amplitude for  $y$  polarization  $r_{yy}$  gradually increases from 0 to nearly 0.9 at the working frequency 14.6 GHz when the sheet resistance of graphene  $R_g$  varies from 800 to  $50 \Omega \square^{-1}$ , while the reflected amplitude for  $x$  polarization  $r_{xx}$  always keeps on exceeding 0.9 at 14.6 GHz. On the other hand, the reflected phase for both  $x$  and  $y$  polarization ( $\phi_{xx}$  and  $\phi_{yy}$ ) are nearly equal to  $\pi$  at 14.6 GHz, showing insensitivity to the sheet resistance  $R_g$ . It should be noted that although  $\phi_{yy}$  changes dramatically when  $R_g$  increases over  $800 \Omega \square^{-1}$ , it has little impact on the final resultant reflected wave due to the weak amplitude response ( $r_{yy}$  close to zero) in this case. Furthermore, Fig. 3c, f depicts the amplitude difference ( $\Delta r$ ) and phase difference ( $\Delta\phi$ ) between co-polarized reflection coefficients for  $x$  and  $y$  polarization, where  $\Delta r = r_{xx} - r_{yy}$  and  $\Delta\phi = \phi_{yy} - \phi_{xx}$ . It is seen in Fig. 3f that the phase difference is exactly equal to 0 at 14.6 GHz in the sheet resistance range from 800 to  $50 \Omega \square^{-1}$ , thereby fulfilling the phase condition required for manipulating the polarization angle of linear polarization. Figure 3c demonstrates a wide range of amplitude modulation from 0 to 0.96 at 14.6 GHz when the sheet resistance of graphene varies from 800 to  $50 \Omega \square^{-1}$ . However, this polarization selective modulation only works in the reflection mode of the proposed meta-device. According to Eqs. (10) and (11), the normalized intensity of the reflected electric field  $|E_r|$  and polarization angle  $\theta_p$  as functions of sheet resistance of graphene are calculated and depicted in Fig. 3g, h. Figure 3g shows that the normalized intensity of the reflected electric field is higher than 0.7 at 14.6 GHz no matter how the sheet resistance varies. It is seen in Fig. 3h that the polarization angle  $\theta_p$  experiences a considerable shift from  $45^\circ$  to  $0^\circ$  when increasing the sheet resistance from 50 to  $800 \Omega \square^{-1}$ . The proposed meta-device shows a tunable range of polarization angle that operates at room temperature ( $T = 300$  K). It should be noted that extremely low or high temperature will deteriorate the polarization performance due to the effect of graphene and ionic liquid (see Supplementary Fig. 2 and Supplementary Note 2). We also simulated amplitude and phase responses of the proposed structure without graphene layers. It is seen in Fig. 3i that the amplitude responses for  $x$  and  $y$  polarization are nearly

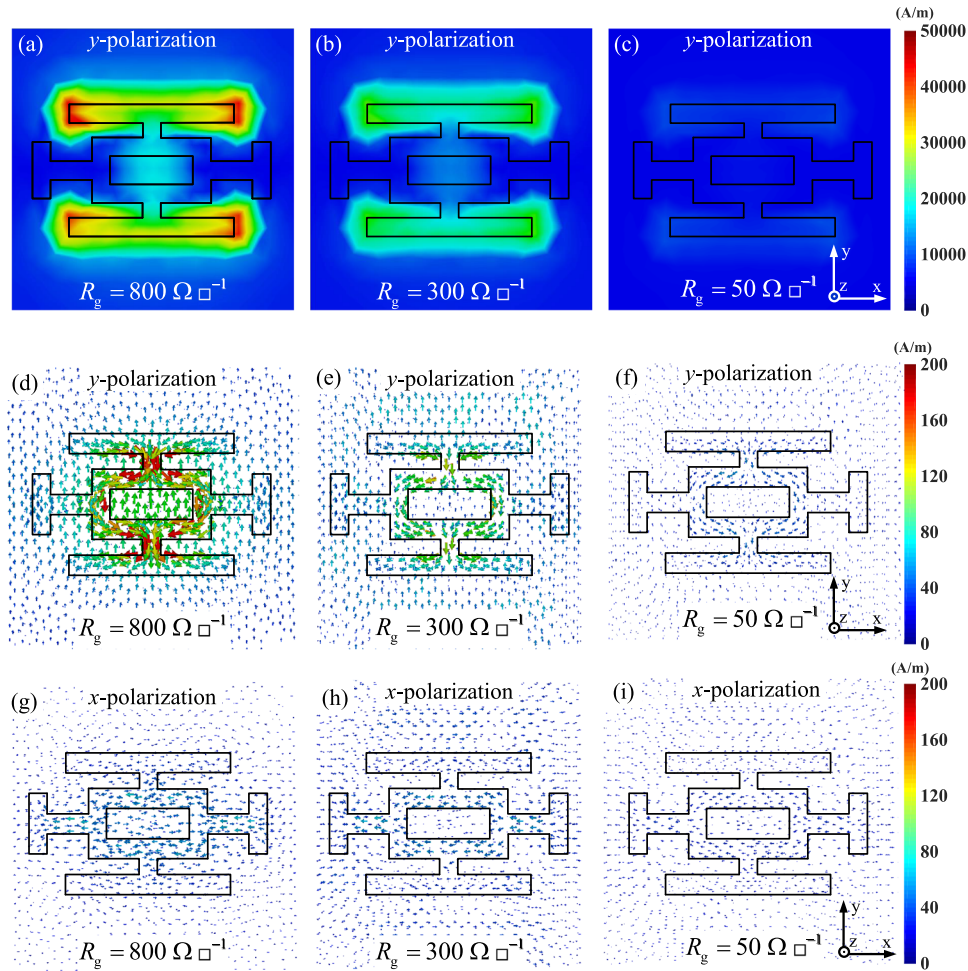


**Fig. 5 Electric fields and induced currents in graphene-based meta-device.** Simulated electric fields (a–c) and induced surface-current distributions (d–f) of the designed meta-device under *y*-polarized incidence with different sheet resistances of 800, 300, and  $50 \Omega \square^{-1}$ . Induced surface-current distributions under *x*-polarized incidence with different sheet resistances of **g**  $800 \Omega \square^{-1}$ , **h**  $300 \Omega \square^{-1}$ , and **i**  $50 \Omega \square^{-1}$ .

equal to 0.9 at the working frequency of 14.6 GHz while the phase difference is about  $110^\circ$ . According to electromagnetic theory, the metallic Jerusalem cross-metasurface only reflects untunable elliptical polarized waves. Compared with this structure, introduction of a graphene layer enables a dynamically tunable anisotropic amplitude response that leads to the polarization rotation of reflected linear waves. Considering a linearly polarized electromagnetic wave with a polarization angle of  $45^\circ$  illuminates onto the graphene-based metasurface, the polarization state of the reflected wave can be dynamically modulated by continuously tuning  $R_g$ .

To further elaborate the operation principle of the proposed meta-device, the device function as a continuous variation of  $R_g$  can be visualized on the fundamental Poincaré sphere as shown in Fig. 4, which is mapped by representing the Stokes parameters in the spherical Cartesian coordinates, defined as<sup>54</sup>:

$$\begin{cases} S_0 = |r_{xx}|^2 + |r_{yy}|^2, \\ S_1 = 2|r_{xx}||r_{yy}| \cos \Delta\varphi, \\ S_2 = 2|r_{xx}||r_{yy}| \sin \Delta\varphi, \\ S_3 = |r_{xx}|^2 - |r_{yy}|^2, \end{cases} \quad (12)$$

Here,  $S_0$  is the unit radius of the Poincaré sphere and  $S_{1,2,3}$  are the sphere's Cartesian coordinates. Therefore, an arbitrary

polarization state can be characterized by one point on the surface of the Poincaré sphere. For instance, the north and south poles represent right and left circular polarization. The equator denotes the azimuthally varying linear polarization, while intermediate points in the northern and southern hemispheres correspond to elliptical polarization. It is seen in Fig. 4 that the variation of  $R_g$  forms a continuous path on the equator of the Poincaré sphere. It starts at the (0,0) and ends near  $(0.5\pi, 0)$ , indicating that the polarization angle of the reflected linear-polarized wave sweeps from  $0^\circ$  to  $45^\circ$  when the sheet resistance of graphene increases from 800 to  $50 \Omega \square^{-1}$ . To validate the performance of polarization modulations, we propose four typical polarization states as examples shown in Fig. 4. The normalized values of electromagnetic energies for *x* and *y* polarizations are presented in green and blue colors, respectively, and the resulting polarization vector is plotted as a red arrow. By shifting the sheet resistance of graphene to 800, 550, 300, and  $50 \Omega \square^{-1}$ , the normalized reflected amplitude for *x* polarization is effectively modulated as 0.01, 0.17, 0.43, and 0.87, while that for *y* polarization remains close to 0.9. Therefore, the polarization angles  $\theta_p$  of the resultant vectors are obtained as  $0.68^\circ$ ,  $10.19^\circ$ ,  $24.89^\circ$ , and  $45^\circ$ . It should be noted that the reflection amplitudes in these cases are all close to 0.7, which shows considerable high efficiency.

In order to get a comprehensive insight into the mechanism of the polarization modulation in our proposed meta-device,

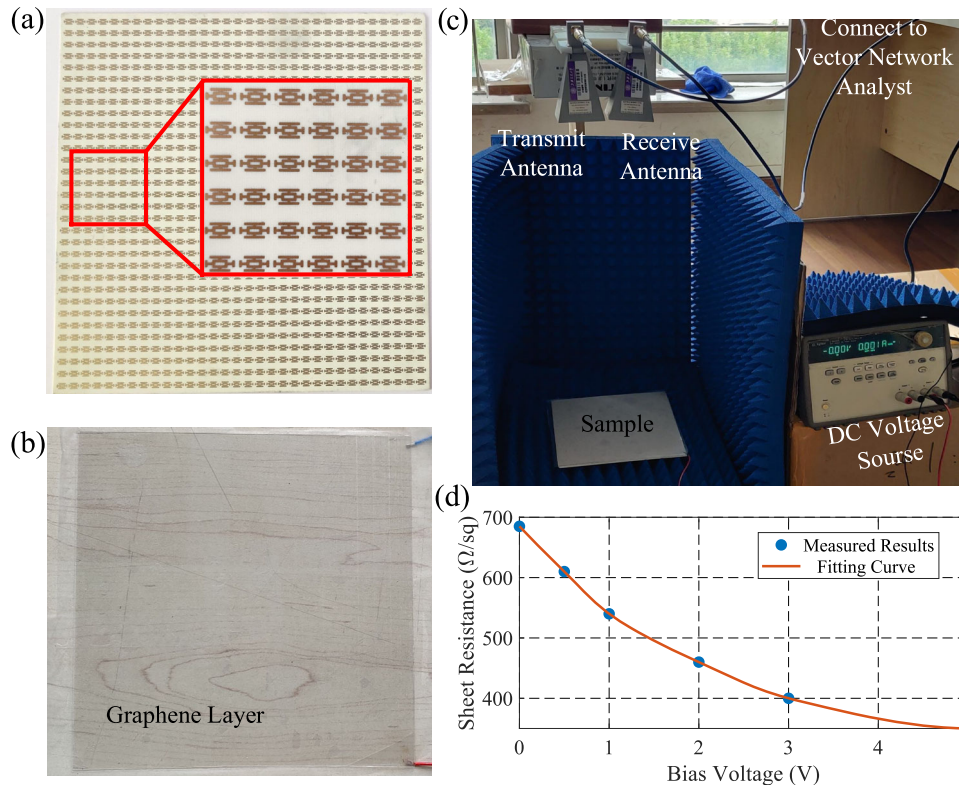


**Fig. 6** **Prototype and measurement setup.** Photograph of **a** patterned metallic layer, **b** graphene-based sandwich structure connected to bias voltage, and **c** measurement setup. **d** Relation between the bias voltage and sheet resistance of graphene.

the distribution of the electric field and surface current on a unit cell of the metal pattern with different sheet resistances of 800, 300, and  $50 \Omega \square^{-1}$  are illustrated in Fig. 5. We consider a y-polarized electromagnetic wave impinges normally on the structure, and the results in Fig. 5a–f are monitored at the working frequency of 14.6 GHz. Figure 5a shows that, for  $R_g = 800 \Omega \square^{-1}$ , the electric fields are strongly concentrated in the upper and lower arms of the metal patterns. Thus, opposite charges accumulate in the adjacent unit cells of meta-devices along the y direction, producing capacitive behaviors. To determine the resonance type (electric or magnetic), the surface-current distributions of the proposed meta-devices are plotted in Fig. 5d. The induced currents are mainly distributed on the connections between long arms and the central square loop, and the directions of current along  $-y$  direction are opposite to that on the top graphene layer and bottom ground plane, which can be considered as the magnetic dipole resonances. The strong resonance can effectively trap the incoming power and provide an opportunity to be dissipated by the graphene losses. Furthermore, the intensities of electric field energy and induced current distributed on the metal pattern are gradually reduced as  $R_g$  decreases and even weakened to be ignored when  $R_g = 50 \Omega \square^{-1}$ . Accordingly, it can be found that the resonance can be controlled by the sheet resistance of graphene that leads to the reflected amplitude modulation. In contrast, the induced surface-current distributions for x polarization illumination have different results. As shown in Fig. 5g–i, it is obviously seen that the induced currents are always weak in any case of  $R_g$ , indicating that no resonance is excited about x polarization. Based on these results, the mechanism of the polarization modulation method we present is fully demonstrated.

### Measurements

To further verify the meta-device performance by experiments, we fabricated a prototype composed of  $32 \times 32$  unit cells, as shown in Fig. 6a, b. The overall size of the prototype is  $192 \times 192 \text{ mm}^2$ . The metallic patterns and ground plate are made of  $17\text{-}\mu\text{m}$ -thick copper etched on both sides of the Rogers 4350b substrate by conventional printed circuit board technique. The measured relation between sheet resistance of graphene and the bias voltage is exhibited in Fig. 6d. It is seen that the sheet resistance of graphene decreases monotonously from nearly 700 to  $350 \Omega \square^{-1}$  while the voltage increases from 0 to 5 V. Furthermore, the responding fitting curve is also provided in Fig. 6d, from which, the approximate values of  $R_g$  under different bias voltage can be obtained easily and rapidly. Besides, the low bias voltage enables avoiding the break-down effect of the dielectric layers such as PET and foam. Measurement of the scattering field is conducted using the free-space wave method<sup>40</sup>, as shown in Fig. 6c.

Figure 7 shows the measured amplitude and phase components of reflection coefficients for both x- and y-polarized incidence. Here, five typical voltages 0, 0.5, 1, 2, 3, and 5 V are applied to graphene layers, corresponding approximately to sheet resistances of 680, 620, 540, 460, 400, and  $340 \Omega \square^{-1}$ , respectively. It is seen in Fig. 7a, c that, at the frequency of 15.3 GHz (blue zone), the measured reflected amplitude for y polarization keeps almost unchanged (less than 1 dB) when gradually increasing the bias voltage  $U$  from 0 to 5 V, while for x polarization the reflected amplitude experiences dramatic shifts. On the other hand, the measured reflected phases for x and y polarizations are all nearly equal to  $10^\circ$  no matter how bias voltage changes as shown in Fig. 7b, d. Therefore, according to Eq. (11), the polarization angle  $\theta_p$  can be experimentally shifted from  $3.72^\circ$  to  $23.34^\circ$ . In detail, the measured polarization angle corresponding to bias voltage of 0, 0.5, 1, 2, 3, and 5 V are  $3.72^\circ$ ,  $7.79^\circ$ ,  $11.71^\circ$ ,  $14.91^\circ$ ,  $18.07^\circ$ , and

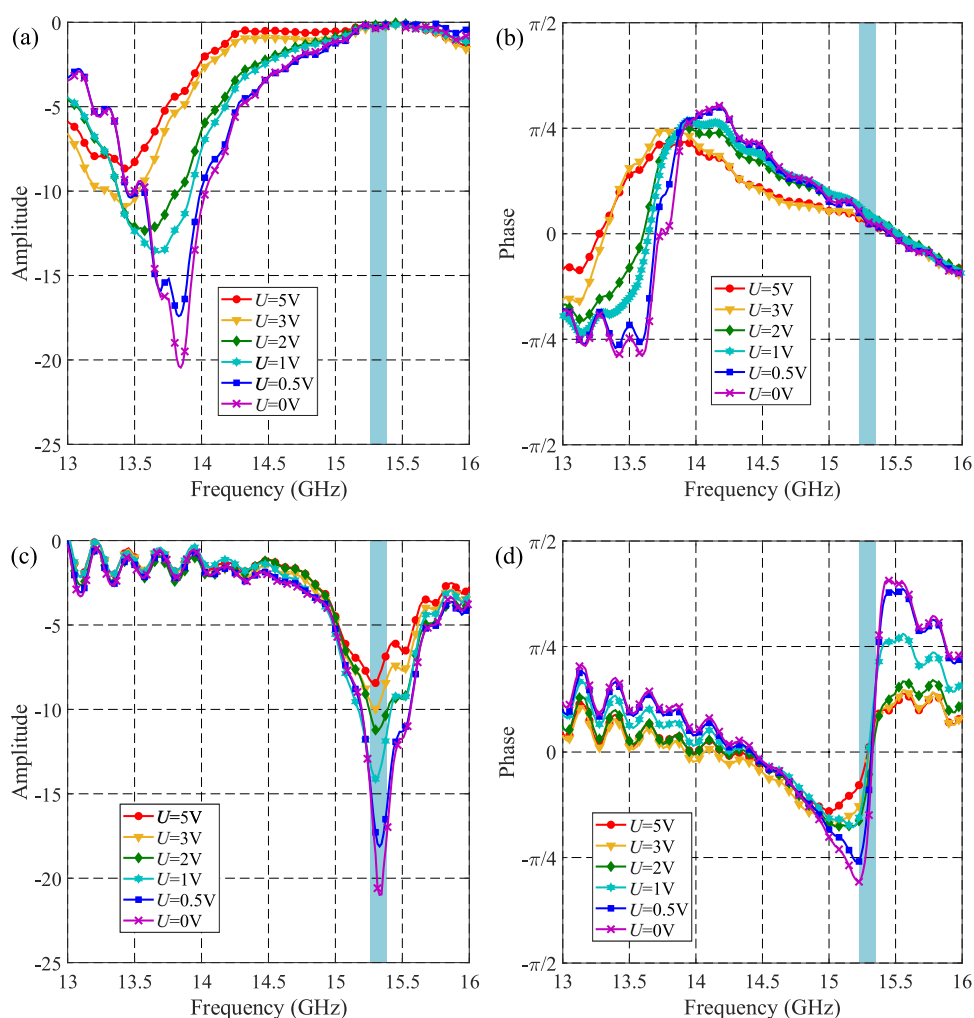


**Fig. 7 Measurement results.** Measured reflected amplitude and phase spectra of the proposed meta-device under **a, b**  $x$ - and **c, d**  $y$ -polarized incidence for different bias voltages of 0–5 V.

23.34°, respectively. The slight deviation between the measured and simulated working frequencies may be caused by the inconsistency in the dielectric constant and thickness of the substrate and foam layers in practice. Besides, the tunable range of polarization angle fails to meet the simulated expectation that is mainly due to the limited range of graphene's sheet resistance available in practical. Although the minimum sheet resistance can be effectively reduced by stacking a multilayer structure, but the maximum value correspondingly decreases either, which makes no sense for improvement of polarization performance (full data are provided in the Supplementary Fig. 3 and Supplementary Note 3). Improving the quality of pristine monolayer graphene and utilizing ionic liquid with a higher ionization degree are two executable solutions for extending the tunable range of graphene's sheet resistance.

In summary, we have experimentally presented a novel design of graphene-based meta-device for dynamical polarization manipulation of electromagnetic waves. In contrast to the conventional scheme of changing the geometrical parameters of the structure or loading active electronic elements such PINs and varactors, graphene is introduced to realize anisotropic amplitude modulation of microwaves operating in a reflective mode in a simpler manner. Therefore, the proposed meta-device is capable of dynamically and continuously rotating polarization angle by applying different bias voltages to graphene layers. The relationship between polarization states and sheet resistance of graphene

has also been analyzed in detail. Our results advance the state-of-the-art polarization manipulation achievable by CVD graphene and represent a step towards real and practical applications of integrated graphene-based devices or systems.

## METHODS

### Fabrication of graphene-based meta-device

Graphene monolayers are synthesized on the 20- $\mu\text{m}$ -thick copper sheet using CVD method and transferred onto the PET substrate through the dry transfer method<sup>55–57</sup>. It is noted that these procedures are finished by Ningbo Soft Carbon Electronic Technology Co., Ltd. Subsequently, a graphene sandwich structure was fabricated consisting of two graphene monolayers on the PET substrate and a diaphragm paper in the middle soaked with ionic liquid as discussed in refs.<sup>48–50</sup>. Finally, the graphene sandwich structure is pasted to the Teflon foam slab, and then aligned together to the metal patterned substrate.

### Setup of measurement

Two standard linearly polarized horn antennas connected to a vector network serve as transmitter and receiver to measure the reflection parameters of the sample. The voltage applied to the graphene layer is offered by a direct current voltage source. The distance between antennas and the sample is set to be far enough to avoid the near-field effect. Before the measurement, calibration was carried out against the open aperture and copper metal plate on the sample holder. This arrangement minimizes measurement errors, such as scattering and diffraction.

## DATA AVAILABILITY

The data are available from the corresponding author upon reasonable request.

## CODE AVAILABILITY

The codes that support the findings of this study are not available in the public domain. However, the authors will be happy to discuss an appropriate accommodation for reasonable requests.

Received: 23 January 2022; Accepted: 10 June 2022;

Published online: 12 July 2022

## REFERENCES

- Yu, N. et al. Light propagation with phase discontinuities: generalized laws of reflection and refraction. *Science* **334**, 333–337 (2011).
- Sun, S. et al. Gradient-index meta-surfaces as a bridge linking propagating waves and surface waves. *Nat. Mater.* **11**, 426–431 (2012).
- Ni, X., Emani, N. K., Kildishev, A. V., Boltasseva, A. & Shalaev, V. M. Broadband light bending with plasmonic nanoantennas. *Science* **335**, 427 (2012).
- Orazbayev, B., Mohammadi Estakhri, N., Alù, A. & Beruete, M. Experimental demonstration of metasurface-based ultrathin carpet cloaks for millimeter waves. *Adv. Opt. Mater.* **5**, 1600606 (2017).
- Li, L. et al. Electromagnetic reprogrammable coding-metasurface holograms. *Nat. Commun.* **8**, 1–7 (2017).
- Li, Z., Premaratne, M. & Zhu, W. Advanced encryption method realized by secret shared phase encoding scheme using a multi-wavelength metasurface. *Nanophotonics* **9**, 3687–3696 (2020).
- Cui, T.-J., Liu, S. & Li, L.-L. Information entropy of coding metasurface. *Light Sci. Appl.* **5**, e16172 (2016).
- Zhao, H. et al. Metasurface-assisted massive backscatter wireless communication with commodity wi-fi signals. *Nat. Commun.* **11**, 1–10 (2020).
- Akram, M. R., Ding, G., Chen, K., Feng, Y. & Zhu, W. Ultrathin single layer metasurfaces with ultra-wideband operation for both transmission and reflection. *Adv. Mater.* **32**, 1907308 (2020).
- Chen, K. et al. Directional janus metasurface. *Adv. Mater.* **32**, 1906352 (2020).
- Wu, J. W. et al. Full-state synthesis of electromagnetic fields using high efficiency phase-only metasurfaces. *Adv. Funct. Mater.* **30**, 2004144 (2020).
- Bao, L. et al. Multi-beam forming and controls by metasurface with phase and amplitude modulations. *IEEE Trans. Antennas Propag.* **67**, 6680–6685 (2019).
- Holliman, N. S., Dodgson, N. A., Favalora, G. E. & Pockett, L. Three-dimensional displays: a review and applications analysis. *IEEE Trans. Broadcast.* **57**, 362–371 (2011).
- Browne, D. E. & Rudolph, T. Resource-efficient linear optical quantum computation. *Phys. Rev. Lett.* **95**, 010501 (2005).
- Tyo, J. S., Goldstein, D. L., Chenault, D. B. & Shaw, J. A. Review of passive imaging polarimetry for remote sensing applications. *Appl. Opt.* **45**, 5453–5469 (2006).
- Huang, C. X., Zhang, J., Cheng, Q. & Cui, T. J. Polarization modulation for wireless communications based on metasurfaces. *Adv. Funct. Mater.* **31**, 2103379 (2006).
- Chen, X. et al. Designing an excellent deep-ultraviolet birefringent material for light polarization. *J. Am. Chem. Soc.* **140**, 16311–16319 (2018).
- Ali, S., Davies, J. R. & Mendonca, J. T. Inverse faraday effect with linearly polarized laser pulses. *Phys. Rev. Lett.* **105**, 035001 (2010).
- Shi, Z. et al. Continuous angle-tunable birefringence with freeform metasurfaces for arbitrary polarization conversion. *Sci. Adv.* **6**, eaba3367 (2020).
- Kang, L. et al. Nonlinear chiral meta-mirrors: enabling technology for ultrafast switching of light polarization. *Nano Lett.* **20**, 2047–2055 (2020).
- Rubin, N. A. et al. Polarization state generation and measurement with a single metasurface. *Opt. Express* **26**, 21455–21478 (2018).
- Rubin, N. A. et al. Matrix fourier optics enables a compact full-stokes polarization camera. *Science* **365**, eaax1839 (2019).
- Deng, Z.-L. et al. Diatomic metasurface for vectorial holography. *Nano Lett.* **18**, 2885–2892 (2018).
- Xu, P., Jiang, W. X., Wang, S. Y. & Cui, T. J. An ultrathin cross-polarization converter with near unity efficiency for transmitted waves. *IEEE Trans. Antennas Propag.* **66**, 4370–4373 (2018).
- Yu, Y., Xiao, F., He, C., Jin, R. & Zhu, W. Double-arrow metasurface for dual-band and dual-mode polarization conversion. *Opt. Express* **28**, 11797–11805 (2020).
- Liu, W. et al. Realization of broadband cross-polarization conversion in transmission mode in the terahertz region using a single-layer metasurface. *Opt. Lett.* **40**, 3185–3188 (2015).
- Zhao, X. et al. Electromechanically tunable metasurface transmission waveplate at terahertz frequencies. *Optica* **5**, 303–310 (2018).
- Dorrah, A. H., Rubin, N. A., Zaidi, A., Tamagnone, M. & Capasso, F. Metasurface optics for on-demand polarization transformations along the optical path. *Nat. Photon* **15**, 287–296 (2021).
- Song, Q. et al. Bandwidth-unlimited polarization-maintaining metasurfaces. *Sci. Adv.* **7**, eabe1112 (2021).
- Ma, Q. et al. Editing arbitrarily linear polarizations using programmable metasurface. *Phys. Rev. Appl.* **13**, 021003 (2020).
- Park, J., Kang, J.-H., Kim, S. J., Liu, X. & Brongersma, M. L. Dynamic reflection phase and polarization control in metasurfaces. *Nano Lett.* **17**, 407–413 (2017).
- Tao, Z., Wan, X., Pan, B. C. & Cui, T. J. Reconfigurable conversions of reflection, transmission, and polarization states using active metasurface. *Appl. Phys. Lett.* **110**, 121901 (2017).
- Song, X., Bai, X. & Zhu, W. Reconfigurable metasurface for nearly full-range and continuous modulation of reflection, transmission, and absorption. *ACS Appl. Electron. Mater.* **4**, 1225–1231 (2022).
- Novoselov, K. S. et al. Electric field effect in atomically thin carbon films. *Science* **306**, 666–669 (2004).
- Geim, A. K. & Novoselov, K. S. The rise of graphene. *Nat. Mater.* **6**, 183–191 (2007).
- Neto, A. H. C., Guinea, F., Peres, N. M. R., Novoselov, K. S. & Geim, A. K. The electronic properties of graphene. *Rev. Mod. Phys.* **81**, 109–162 (2009).
- Guo, T. & Argyropoulos, C. Broadband polarizers based on graphene metasurfaces. *Opt. Lett.* **41**, 5592–5595 (2016).
- Cheng, H. et al. Mid-infrared tunable optical polarization converter composed of asymmetric graphene nanocrosses. *Opt. Lett.* **38**, 1567–1569 (2013).
- Khorasani, S. & Koottandavida, A. Nonlinear graphene quantum capacitors for electro-optics. *npj 2D Mater. Appl.* **1**, 7 (2017).
- Zhang, Y. et al. Tunable broadband polarization rotator in terahertz frequency based on graphene metamaterial. *Carbon* **133**, 170–175 (2018).
- Jung, M. et al. Polarimetry using graphene-integrated anisotropic metasurfaces. *ACS Photonics* **5**, 4283–4288 (2018).
- Zhang, J. & Zhu, W. Graphene-based microwave metasurfaces and radio-frequency devices. *Adv. Photonics Res.* **2**, 2100142 (2021).
- Chen, H., Lu, W.-B., Liu, Z.-G. & Jiang, Z. H. Flexible rasorber based on graphene with energy manipulation function. *IEEE Trans. Antennas Propag.* **68**, 351–359 (2020).
- Chen, H. et al. Microwave beam reconfiguration based on graphene ribbon. *IEEE Trans. Antennas Propag.* **66**, 6049–6056 (2018).
- Grande, M. et al. Optically transparent microwave polarizer based on quasi-metallic graphene. *Sci. Rep.* **5**, 17083 (2015).
- Chen, H., Liu, Z., Lu, W., Zhang, A. & Jiang, Z. H. Full polarization transformation using graphene in microwave frequencies. *IEEE Trans. Antennas Propag.* **68**, 3760–3769 (2020).
- Zhang, C. et al. Graphene-based anisotropic polarization meta-filter. *Mater. Des.* **206**, 109768 (2021).
- Chen, H., Lu, W.-B., Liu, Z.-G. & Geng, M.-Y. Microwave programmable graphene metasurface. *ACS Photonics* **7**, 1425–1435 (2020).
- Balci, O., Polat, E. O., Kakenov, N. & Kocabas, C. Graphene-enabled electrically switchable radar-absorbing surfaces. *Nat. Commun.* **6**, 6628 (2015).
- Zhang, J., Wei, X., Rukhlenko, I. D., Chen, H.-T. & Zhu, W. Electrically tunable metasurface with independent frequency and amplitude modulations. *ACS Photonics* **7**, 265–271 (2020).
- Hanson, G. W. Dyadic green's functions and guided surface waves for a surface conductivity model of graphene. *J. Appl. Phys.* **103**, 064302 (2008).
- Zhang, X., Hu, H., Lin, X., Shen, L. & Chen, H. Confined transverse-electric graphene plasmons in negative refractive-index systems. *npj 2D Mater. Appl.* **4**, 25 (2020).
- Menzel, C. et al. Asymmetric transmission of linearly polarized light at optical metamaterials. *Phys. Rev. Lett.* **104**, 253902 (2010).
- Milione, G., Sztul, H. I., Nolan, D. A. & Alfano, R. R. Higher-order poincaré sphere, stokes parameters, and the angular momentum of light. *Phys. Rev. Lett.* **107**, 053601 (2011).
- Wang, D.-Y. et al. Clean-lifting transfer of large-area residual-free graphene films. *Adv. Mater.* **25**, 4521–4526 (2013).
- Juang, Z.-Y. et al. Graphene synthesis by chemical vapor deposition and transfer by a roll-to-roll process. *Carbon* **48**, 3169–3174 (2010).
- Kang, J. et al. Efficient transfer of large-area graphene films onto rigid substrates by hot pressing. *ACS Nano* **6**, 5360–5365 (2012).

## ACKNOWLEDGEMENTS

This work was supported by the National Natural Science Foundation of China (NSFC) (62071291). The authors acknowledge support in part from the Center for Advanced Electronic Materials and Devices of Shanghai Jiao Tong University.



## AUTHOR CONTRIBUTIONS

The idea and experiment were conceived by J.Z. and W.Z.; data analysis was done by Z.L., C.Z., and L.S. All authors discussed the results and participated in the writing of the manuscript.

## COMPETING INTERESTS

The authors declare no competing interests.

## ADDITIONAL INFORMATION

**Supplementary information** The online version contains supplementary material available at <https://doi.org/10.1038/s41699-022-00322-8>.

**Correspondence** and requests for materials should be addressed to Weiren Zhu.

**Reprints and permission information** is available at <http://www.nature.com/reprints>

**Publisher's note** Springer Nature remains neutral with regard to jurisdictional claims in published maps and institutional affiliations.



**Open Access** This article is licensed under a Creative Commons Attribution 4.0 International License, which permits use, sharing, adaptation, distribution and reproduction in any medium or format, as long as you give appropriate credit to the original author(s) and the source, provide a link to the Creative Commons license, and indicate if changes were made. The images or other third party material in this article are included in the article's Creative Commons license, unless indicated otherwise in a credit line to the material. If material is not included in the article's Creative Commons license and your intended use is not permitted by statutory regulation or exceeds the permitted use, you will need to obtain permission directly from the copyright holder. To view a copy of this license, visit <http://creativecommons.org/licenses/by/4.0/>.

© The Author(s) 2022